ELSEVIER

Comput. Methods Appl. Mech. Engrg. 149 (1997) 49–71

Computer methods in applied mechanics and engineering

On the choice of finite rotation parameters

Adnan Ibrahimbegovic

Compiègne University of Technology, UTC, Dept. GSM, Division MNM, BP-529, 60206 Compiègne, France

Dedicated to Prof. J. Tinsley Oden for his 60th birthday

Abstract

In this work we discuss some aspects of the three-dimensional finite rotations pertinent to the formulation and computational treatment of the geometrically exact structural theories. Among various possibilities to parameterize the finite rotations, special attention is dedicated to a choice featuring an incremental rotation vector. Some computational aspects pertinent to the implementation of the Newton iterative scheme and the Newmark time-stepping algorithm applied to solving these problems are examined. Representative numerical simulations are presented in order to illustrate the performance of the proposed formulation.

0. Dedication

Current strong interest in nonlinear analysis of physics phenomena, nourished by ever-growing computational resources, has long been anticipated by J. Tinsley Oden. In the early 1970s he published a book (see [1]), which served as a road-map for many developments which followed. In this and later works, Dr. Oden recognized that the proper setting for these developments is placed at the cross-roads between nonlinear mechanics theories and numerical analysis, helping to establish an independent identity of the scientific discipline of Computational Mechanics. In particular, I have always appreciated a distinct style and mathematical rigor of Tinsley's works, which I believe is the only way to make headway in nonlinear problems. I personally benefited from many works of Tinsley Oden, starting from my PhD thesis at UC Berkeley in the late 1980s, where the contact model proposed by Oden and Martins [2] proved very useful for structure–foundation interaction problems I was studying at the time. I am also pleased that my contribution selected for this occasion, regarding some computational aspects in structural theories with finite rotations, appears to be related to a very recent work of Tinsley (see [3]) with an ambitious goal of placing these structural theories in a proper harmony with classical continuum theories and delegating some of the traditional engineer's responsibilities to an adaptive modeling procedure.

1. Introduction

A fascinating subject of finite rotations has intrigued the applied mathematics research community ever since the fundamental works of Euler, Hamilton and Rodrigues (see e.g. [4], for the history overview) culminating with the currently most often invoked description in terms of a special Lie group of orthogonal 3d tensors, SO(3) (see e.g. [5]). In the computational mechanics community, initial interest in the finite rotations was stirred by the work of Argyris [6]. However, it was only with the recent development of the so-called geometrically exact structural theories (see e.g. [7–9] or [10]), which make use of finite rotations (rotations not restricted in

PII S0045-7825(97)00059-5

size), that the urgent need has arisen to address the pertinent computational issues. Several representative works proposing the computational procedures appropriate for this class of problems are given by Simo and Vu-Quoc [11], Cardona and Geradin [12], Sansour and Bufler [13], Buechter and Ramm [14] or Ibrahimbegovic et al. [15], among others.

Various possibilities for selecting the parameters for finite rotation representation (see e.g. review in [16]) are placed between two extreme choices: on one hand, the nine-parameter intrinsic representation by an orthogonal tensor, and on the other hand the three-parameter representation by the so-called rotation vector (see e.g. [15]). Each of these two extremes has certain deficiencies: the former, with a large number of parameters to handle, being computationally expensive and leading to a non-symmetric tangent operator (see e.g. [6]), and the latter not being singularity-free in the global sense.[1] The intrinsic representation of the finite rotations by an orthogonal tensor can be reduced to four quaternion parameters (see e.g. [6] or [16]), which renders the associated computational procedure more efficient by replacing the matrix multiplication by the quaternion algebra;[2] However, the consistent tangent remains non-symmetric.

The main thrust in this work is directed towards a development of a method which eliminates the deficiencies alluded to in the above, and which appears not to have been previously discussed even in the most recent reviews on the subject (see e.g. [17] or [18]). The main idea stems from our previous work (see [15]) where a vector-like parameterization is proposed which always leads to the symmetric tangent form. However, as opposed to that work where the vector parameters are defined in the global sense, in this work we consider *incremental* vector-like rotation parameters. As the major consequence of such a choice, we not only obtain the symmetric form of the tangent operator, but also remove the singularity of the vector-like parameterization and the associated ill-conditioning problem. All this is accomplished simply by restricting the size of the incremental rotation. The latter does not represent additional burden on the solution procedure introduced by the proposed approach, since the same kind of restriction is already implied in ensuring the convergence properties of a typical iterative scheme.

Another advantage of the proposed incremental vector parameterization of finite rotations becomes apparent when we discuss the implementation of time-stepping schemes for the dynamics of structures undergoing finite rotations. We can construct a logical extension of the classical Newmark time-stepping algorithm with incremental rotation vector playing a key role. The simplicity of the present development is in sharp contrast with complexities encountered when one tries using orthogonal tensor parameterization of finite rotations for the same purpose.

The outline of the paper is as follows. In the next section we present the governing equations for statics and dynamics of the chosen model problem, the geometrically exact beam theory accounting for finite rotations. In Section 3, we briefly discuss the vector-like parameterization of finite rotations and present some interesting observations regarding the relationship of that parameterization and the intrinsic one employing the orthogonal tensor. In Section 4, we discuss the advocated choice of the rotation parameters, the incremental rotation vector, its use in an iterative solution procedure and in time-stepping schemes. Several illustrative numerical simulations are given in Section 5, and some concluding remarks are made in Section 6.

2. Three-dimensional geometrically exact beam

2.1. Local form of governing equations

We consider the model problem of three-dimensional beam undergoing the large displacements and rotations. The beam balance equations can be obtained without introducing any simplifying hypothesis regarding its geometry or displacement and rotation size—therefore this beam theory is referred to as the *geometrically exact*

[1] This is a well-known result already established for Euler's angles and all other three-parameters representations (see e.g. [19]).

[2] The computational procedure can be formulated in terms of quaternions in such a way (see e.g. [20]) that the most sensitive step of extracting the corresponding quaternion parameters from a given rotation matrix (see e.g. [21]) is completely by-passed, which is in sharp contrast with the previously proposed computational schemes (see e.g. [6] or [11]).

(see e.g. [7] or [10], and [23] for a 2d case). The linear and angular momentum balance can be written, respectively, as

$$\dot{\boldsymbol{p}} = \boldsymbol{n}' + \bar{\boldsymbol{n}} \tag{1}$$

and

$$\dot{\boldsymbol{r}} = \boldsymbol{m}' + \boldsymbol{\chi}' \times \boldsymbol{n} + \bar{\boldsymbol{m}} \,, \tag{2}$$

where $\boldsymbol{p}$ and $\boldsymbol{r}$ are, respectively, linear and angular momenta, $\boldsymbol{n}$ and $\boldsymbol{m}$ are internal stress resultants, and $\bar{\boldsymbol{n}}$ and $\bar{\boldsymbol{m}}$ are external forces and couples. All the forces act in the current configuration, but are parameterized by the arc-length s of the reference configuration (see Fig. 1). In (1), (2) and in the foregoing, we use prime to denote the partial derivative with respect to the arc-length parameter and superposed dot to denote the partial derivative with respect to time, i.e. $(\bullet)' \equiv \partial/\partial s(\bullet)$ and $(\dot{\bullet}) \equiv \partial/\partial t(\bullet)$, and '$\times$' to denote the vector product.

The beam deformed configuration is defined by a position vector $\boldsymbol{x} = (\boldsymbol{\chi}_0)$ (see Fig. 1) and the new placement of the local Cartesian frame $\boldsymbol{a}_{0i}$, which is constructed in the initial configuration so that one of its unit vectors is perpendicular to the cross section. In accordance with the fundamental kinematic hypothesis (see e.g. [23]), that the plane sections remain plane, this unit vector remains perpendicular to the cross section in the deformed configuration (see Fig. 1). Tensor $\boldsymbol{\Lambda}$ which maps one unit vector into another unit vector must be orthogonal, i.e.

$$\boldsymbol{a} = \boldsymbol{\Lambda}\boldsymbol{a}_0 \,; \qquad \|\boldsymbol{a}\| = \|\boldsymbol{a}_0\| \,; \qquad \Rightarrow \boldsymbol{\Lambda}^{\mathrm{T}}\boldsymbol{\Lambda} = \boldsymbol{I} \,. \tag{3}$$

Moreover, since $\boldsymbol{\Lambda}$ takes one vector in the initial configuration into another vector in the deformed configuration, $\boldsymbol{\Lambda}$ is also a two-point tensor (see e.g. [24]) defined as

$$\begin{aligned} \boldsymbol{\Lambda} &= \boldsymbol{a}_i \otimes \boldsymbol{a}_{0i} \\ &= \bar{\Lambda}_{ij} \boldsymbol{e}_j \otimes \boldsymbol{e}_{0i} \,, \end{aligned} \tag{4}$$

where $\bar{\Lambda}_{ij}$ is its coordinate representation in the global coordinate systems of the reference and the current configurations, with $\boldsymbol{e}_{0i}$ and $\boldsymbol{e}_i$ as the corresponding base vectors. In (4) above and in the foregoing, we use '$\otimes$' to denote the tensor product of vectors. We note in passing that although the base vectors of two global coordinate systems are chosen to coincide (see Fig. 1), the different symbols are retained for clarity. Hence, using a unit, two-point tensor $\boldsymbol{I}$, we can write

$$\boldsymbol{e}_i = \boldsymbol{I}\boldsymbol{e}_{0i} \Rightarrow \boldsymbol{I} = \boldsymbol{e}_i \otimes \boldsymbol{e}_{0i} \,. \tag{5}$$

One can show (see e.g. [20]) that the vector form of the (finite) strain measures, energy-conjugate to the stress resultants and couples, can be obtained as

$$\boldsymbol{\epsilon} = \boldsymbol{\chi}' - \boldsymbol{a} \tag{6}$$

and

$$\boldsymbol{\kappa} = \boldsymbol{\omega} \,, \tag{7}$$

where $\boldsymbol{\epsilon}$ contains the axial and shear strains and $\boldsymbol{\kappa}$ are the bending strains. In (7), $\boldsymbol{\omega}$ is the axial vector of the skew-symmetric tensor $\boldsymbol{\Omega}$ defined as

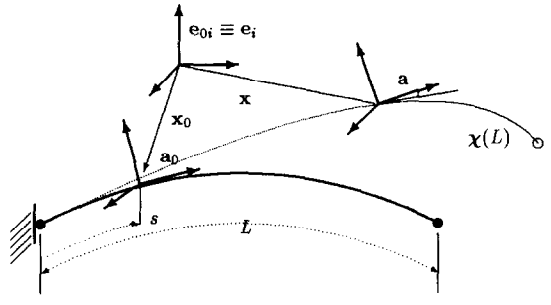

Fig. 1. Three-dimensional beam: initial and current configurations.

$$\boldsymbol{\Omega} = \boldsymbol{\Lambda}'\boldsymbol{\Lambda}^{\mathrm{T}}; \qquad \boldsymbol{\Omega b} = \boldsymbol{\omega} \times \boldsymbol{b}; \quad \forall \boldsymbol{b} \in \mathbb{R}^3. \tag{8}$$

The skew-symmetry of tensor $\boldsymbol{\Omega}$ follows directly from its definition in (8) and the orthogonality of $\boldsymbol{\Lambda}$.

The stress resultants are related to the finite strain measures in (6) and (7) through the set of constitutive equations which can be written as

$$\boldsymbol{n} = \boldsymbol{\Lambda C \Lambda}^{\mathrm{T}} \boldsymbol{\epsilon}; \qquad \boldsymbol{C} = \mathrm{diag}(EA, GA_2, GA_3) \tag{9}$$

and

$$\boldsymbol{m} = \boldsymbol{\Lambda D \Lambda}^{\mathrm{T}} \boldsymbol{\kappa}; \qquad \boldsymbol{D} = \mathrm{diag}(GJ, EI_2, EI_3). \tag{10}$$

In summary of these considerations we can say that the position vector $\boldsymbol{\chi}$ and finite rotation tensor $\boldsymbol{\Lambda}$ uniquely define the strain measures in (6) and (7), and the stress resultants in (9) and (10). In other words, the configuration space of the three-dimensional beam can be presented as

$$\mathscr{C} := \{(\boldsymbol{\chi}, \boldsymbol{\Lambda}): [0, L] \times [0, T] \mapsto \mathbb{R}^3 \times \mathrm{SO}(3)\}, \tag{11}$$

where SO(3) is a special orthogonal group, a classical example of one parameter Lie group (see e.g. [5])

$$\mathrm{SO}(3) = \{\boldsymbol{\Lambda}: \mathbb{R}^3 \to \mathbb{R}^3 \mid \boldsymbol{\Lambda}^{\mathrm{T}}\boldsymbol{\Lambda} = \boldsymbol{I}, \det \boldsymbol{\Lambda} = 1\}. \tag{12}$$

REMARK 1. The configuration space of the geometrically exact beam theory is shared by other structural theories; in particular, geometrically exact shell theory with drilling rotations (see [8]) and 3d finite elasticity with independent rotation field (see [9]). Hence, considerations to follow directly apply to these model problems. □

2.2. Beam momenta, angular velocities and accelerations

The principal difficulty introduced by such a parameterization is due to the fact that SO(3) is not a linear space (it is rather a manifold), hence the issues pertinent to the theoretical formulation, consistent linearization and update procedure become more complex. For example, given two successive finite rotations, $\boldsymbol{\Lambda}_1$ and $\boldsymbol{\Lambda}_2$, the proper update procedure which yields the total rotation $\boldsymbol{\Lambda}$ is given as

$$\boldsymbol{\Lambda} = \boldsymbol{\Lambda}_2 \boldsymbol{\Lambda}_1. \tag{13}$$

When superposing an infinitesimal rotation given by a skew-symmetric tensor $\boldsymbol{W}$ and existing finite rotation $\boldsymbol{\Lambda}$, we first need to map $\boldsymbol{W}$ onto SO(3) manifold by means of the exponential mapping (see e.g. [5]) given by the Rodrigues formula (see e.g. [4] for historical aspects) as

$$\exp[\boldsymbol{W}] := \cos w\, \boldsymbol{I} + \frac{\sin w}{w} \boldsymbol{W} + \frac{1 - \cos w}{w^2} \boldsymbol{w} \otimes \boldsymbol{w}; \quad w = \|\boldsymbol{w}\|, \tag{14}$$

where $\boldsymbol{w}$ is the axial vector of tensor $\boldsymbol{W}$, i.e. $\boldsymbol{Wb} = \boldsymbol{w} \times \boldsymbol{b}$, $\forall\, b \in \mathbb{R}^3$.

This kind of superposition procedure is used to compute time derivative of $\boldsymbol{\Lambda}$. In that case, with $\boldsymbol{W}$ the angular velocity at $\boldsymbol{\Lambda}$, we have

$$\begin{aligned} \dot{\boldsymbol{\Lambda}} &= \left.\frac{\partial}{\partial t}\right|_{t=0} [\boldsymbol{\Lambda}_t] \\ &= \left.\frac{\partial}{\partial t}\right|_{t=0} [\exp(t\boldsymbol{W})\boldsymbol{\Lambda}] \\ &= \boldsymbol{W}\boldsymbol{\Lambda}. \end{aligned} \tag{15}$$

One can say that the exponential mapping maps a line ($t\boldsymbol{W}$), located in the tangent space $T_{\Lambda}\mathrm{SO}(3)$ of the Lie group SO(3) at point $\boldsymbol{\Lambda}$, into the one parameter subgroup $\exp(t\boldsymbol{W})$, which is further superposed to $\boldsymbol{\Lambda}$ in order to obtain the final rotation $\boldsymbol{\Lambda}_t$; see Fig. 2 for graphic illustration.

Angular velocity $\boldsymbol{W}$ is a spatial tensor field, since from the last expression and orthogonality of $\boldsymbol{\Lambda}$ it follows that

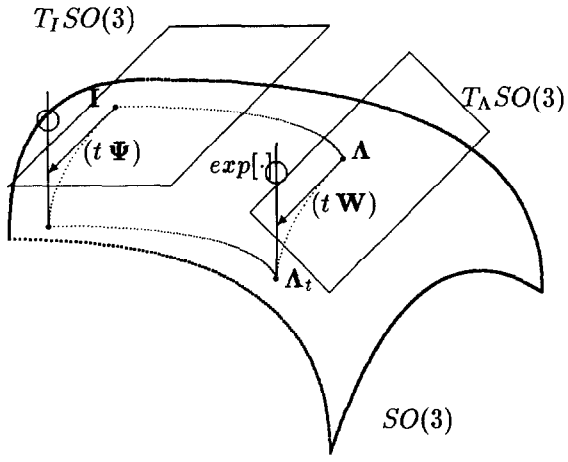

Fig. 2. Angular velocity - material and spatial representation.

$$\begin{aligned} \boldsymbol{W} &= \dot{\boldsymbol{\Lambda}}\boldsymbol{\Lambda}^{\mathrm{T}} \\ &= W_{ij}\boldsymbol{e}_i \otimes \boldsymbol{e}_j \,. \end{aligned} \tag{16}$$

Since $\boldsymbol{\Lambda}$ is a two-point tensor, we can also construct a material representation of its time derivative. Namely, using the material angular velocity $\boldsymbol{\Psi}$, an element of the tangent space $T_1\mathrm{SO}(3)$, defined as

$$\begin{aligned} \boldsymbol{\Psi} &= \boldsymbol{\Lambda}^{\mathrm{T}}\dot{\boldsymbol{\Lambda}} \\ &= \Psi_{ij}\boldsymbol{e}_{0i} \otimes \boldsymbol{e}_{0j} \,, \end{aligned} \tag{17}$$

we can compute an alternative form of this time derivative as

$$\begin{aligned} \dot{\boldsymbol{\Lambda}} &= \frac{\partial}{\partial t}\bigg|_{t=0} [\boldsymbol{\Lambda}_t] \\ &= \frac{\partial}{\partial t}\bigg|_{t=0} [\boldsymbol{\Lambda}\exp(t\boldsymbol{\Psi})] \\ &= \boldsymbol{\Lambda}\boldsymbol{\Psi} \,. \end{aligned} \tag{18}$$

The graphic illustration of this construction is given in Fig. 2.

From two expressions for $\dot{\boldsymbol{\Lambda}}$ in (15) and (18), it readily follows that we can establish the mutual relationship between the material and spatial angular velocities

$$\begin{aligned} \boldsymbol{W} &= \boldsymbol{\Lambda}\boldsymbol{\Psi}\boldsymbol{\Lambda}^{\mathrm{T}} \\ \boldsymbol{\Psi} &= \boldsymbol{\Lambda}^{\mathrm{T}}\boldsymbol{W}\boldsymbol{\Lambda} \,, \end{aligned} \tag{19}$$

which can also be expressed by their axial vectors

$$\begin{aligned} \boldsymbol{w} &= \boldsymbol{\Lambda}\boldsymbol{\psi} \\ \boldsymbol{\psi} &= \boldsymbol{\Lambda}^{\mathrm{T}}\boldsymbol{w} \,, \end{aligned} \tag{20}$$

where $\boldsymbol{\Psi b} = \boldsymbol{\psi} \times \boldsymbol{b}$, $\forall\, \boldsymbol{b} \in \mathbb{R}^3$.

By taking the time derivative of the expressions in (15) and (18) we get, respectively, the angular acceleration field in the spatial

$$\dot{\boldsymbol{W}} = \ddot{\boldsymbol{\Lambda}}\boldsymbol{\Lambda}^{\mathrm{T}} + \dot{\boldsymbol{\Lambda}}\dot{\boldsymbol{\Lambda}}^{\mathrm{T}} \tag{21}$$

and material representation

$$\dot{\boldsymbol{\Psi}} = \boldsymbol{\Lambda}^{\mathrm{T}}\ddot{\boldsymbol{\Lambda}} + \dot{\boldsymbol{\Lambda}}^{\mathrm{T}}\dot{\boldsymbol{\Lambda}} \,. \tag{22}$$

It can be easily verified that angular acceleration tensors $\dot{\boldsymbol{W}}$ and $\dot{\boldsymbol{\Psi}}$ are both skew-symmetric, and that their mutual relationship can be written as

$$\begin{aligned} \dot{\boldsymbol{W}} &= \boldsymbol{\Lambda}\dot{\boldsymbol{\Psi}}\boldsymbol{\Lambda}^{\mathrm{T}} \\ \dot{\boldsymbol{\Psi}} &= \boldsymbol{\Lambda}^{\mathrm{T}}\dot{\boldsymbol{W}}\boldsymbol{\Lambda} . \end{aligned} \tag{23}$$

The latter gives rise to the corresponding relationship between their axial vectors as

$$\begin{aligned} \dot{\boldsymbol{w}} &= \boldsymbol{\Lambda}\dot{\boldsymbol{\psi}} \\ \dot{\boldsymbol{\psi}} &= \boldsymbol{\Lambda}^{\mathrm{T}}\dot{\boldsymbol{w}} . \end{aligned} \tag{24}$$

We note in passing that $\dot{\boldsymbol{\psi}}$ (just like $\boldsymbol{\psi}$) is the element of the tangent space $T_I\mathrm{SO}(3)$, whereas $\dot{\boldsymbol{w}}$ (like $\boldsymbol{w}$) is the element of the tangent space $T_\Lambda\mathrm{SO}(3)$ (see Fig. 2).

With these results on hand, we can write explicit expressions for linear and angular momenta as

$$\boldsymbol{p} = A_\rho\dot{\boldsymbol{\chi}} ; \qquad \boldsymbol{r} = \boldsymbol{I}_\rho\boldsymbol{w} ; \qquad \boldsymbol{I}_\rho = \boldsymbol{\Lambda}\boldsymbol{J}_\rho\boldsymbol{\Lambda}^{\mathrm{T}} , \tag{25}$$

where A_ρ is the mass density per unit length of beam, and $\boldsymbol{J}_\rho$ is inertial dyadic of the beam in material representation.

The time derivative of the beam momenta, appearing in balance equations in (1) and (2), can be computed as

$$\begin{aligned} \dot{\boldsymbol{p}} &= A_\rho\ddot{\boldsymbol{\chi}} ; \\ \dot{\boldsymbol{r}} &= \boldsymbol{I}_\rho\dot{\boldsymbol{w}} + \boldsymbol{w}\times\boldsymbol{I}_\rho\boldsymbol{w} . \end{aligned} \tag{26}$$

2.3. Integral form of balance equations

The momentum balance equations in (1) and (2) can also be written in an integral form, by appealing to the virtual power method (see e.g. [25]) and pairing the stress resultants and couples with their conjugate strain rates. In order to obtain an objective time derivative of the spatial strain measures defined in (6) and (7), we employ the Lie derivative formalism (see e.g. [26]): the objective rate of a vector field is computed with the subsequent applications of the pull-back of the spatial vector field to the reference configuration, the time derivative computation and the push-forward of the resulting expression to the current configuration. In a particular case under consideration, the pull-back and push-forward are carried out by the two-point tensor $\boldsymbol{\Lambda}$ to get

$$L_w[(\bullet)] = \boldsymbol{\Lambda}\frac{\mathrm{d}}{\mathrm{d}t}\bigg|_{t=0}[\boldsymbol{\Lambda}_t^{\mathrm{T}}(\bullet)_t] . \tag{27}$$

The objective strain rates computed in this manner for the axial and shear strains are

$$L_w[\boldsymbol{\epsilon}] = \dot{\boldsymbol{\chi}}' - \boldsymbol{w}\times\boldsymbol{\chi}' . \tag{28}$$

whereas for the bending strains we get

$$L_w[\boldsymbol{\kappa}] = \dot{\boldsymbol{\omega}} - \boldsymbol{w}\times\boldsymbol{\omega} . \tag{29}$$

With these results on hand, the integral form of the balance equations can be written as

$$\begin{aligned} G(\boldsymbol{\chi}, \boldsymbol{\Lambda}, \dot{\boldsymbol{\chi}}, \boldsymbol{w}) := & \int_{[0,L]}\{\dot{\boldsymbol{\chi}}\cdot\dot{\boldsymbol{p}} + \boldsymbol{w}\cdot\dot{\boldsymbol{r}}\}\,\mathrm{d}s \\ & + \int_{[0,L]}\{L_w[\boldsymbol{\epsilon}]\cdot\boldsymbol{n} + L_w[\boldsymbol{\kappa}]\cdot\boldsymbol{m}\}\,\mathrm{d}s + G_{\mathrm{ext}} = 0 , \end{aligned} \tag{30}$$

where G_{ext} represents the virtual power of external forces and couples.

3. Vector-like parameterization of finite rotations

3.1. Motivation: Basic difficulty

The presence of the SO(3) manifold in the configuration space of the beam is the source of the major difficulty in the computational treatment of this problem. More precisely, the update procedure of the rotation leads to rather a costly multiplication and the tangent operator is not symmetric (see e.g. [6] or [11]) which further increases the computational cost.

The first inconvenience can be alleviated by replacing the multiplication of the orthogonal tensors representing the existing and the incremental rotations by quaternion algebra. Namely the existing rotation can be represented by a set of *quaternions*, $\{q_0, \boldsymbol{q}\}$, which gives a four parameter representation of an orthogonal tensor $\boldsymbol{\Lambda}$ as

$$\boldsymbol{\Lambda} = (2q_0^2 - 1)\boldsymbol{I} + 2q_0(\boldsymbol{q}\times) + 2\boldsymbol{q}\otimes\boldsymbol{q}\,. \tag{31}$$

Similarly, with the quaternion parameters for the incremental rotation tensors given as $\{p_0, \boldsymbol{p}\}$, the multiplicative update of the orthogonal tensors can be carried out directly in terms of the quaternion parameters

$$\begin{aligned} q_0 &\leftarrow p_0 q_0 - \boldsymbol{p}\cdot\boldsymbol{q} \\ \boldsymbol{q} &\leftarrow p_0\boldsymbol{q} + q_0\boldsymbol{p} + \boldsymbol{p}\times\boldsymbol{q}\,. \end{aligned} \tag{32}$$

The second deficiency of the intrinsic parameterization of the finite rotations, the non-symmetry of the tangent operator, can be eliminated in some cases (e.g. excluding non-conservative loads) simply by symmetrizing it (see e.g. [7] for justification).

Another method considers a more radical change (e.g., see [15]) by replacing the orthogonal tensor $\boldsymbol{\Lambda}$ in the configuration space by the so-called *rotation vector* $\boldsymbol{\theta}$. Although this method does not lead to a universally acceptable solution, suffering from ill-conditioning problem when the norm of the rotation vector is in the neighborhood of 2π (see e.g. [15]), it is still of interest for the choice of rotation parameters advocated in this work. For that reason, we briefly recall in the foregoing the pertinent considerations of Ibrahimbegovic et al. [15].

3.2. Rotation vector

According to the Euler theorem (see e.g. [27, p. 158]), in each finite rotation there exists a vector $\boldsymbol{\theta}$ that remains invariant under rotation, or in other words, that remains the same when multiplied by the corresponding orthogonal tensor $\boldsymbol{\Lambda}$. In the case under consideration, with $\boldsymbol{\Lambda}$ being a two-point tensor, the latter should be written as

$$\begin{aligned} \boldsymbol{\theta} &= \boldsymbol{\Lambda}\boldsymbol{\vartheta} \\ &= \boldsymbol{I}\boldsymbol{\vartheta}\,, \end{aligned} \tag{33}$$

where $\boldsymbol{\theta}$ is the spatial vector field corresponding to a material vector field $\boldsymbol{\vartheta}$. For the given choice of the global coordinate systems in the reference and the current configurations (see Fig. 1), the components of those two vectors coincide, i.e.

$$\boldsymbol{\theta}\cdot\boldsymbol{e}_i = \boldsymbol{\vartheta}\cdot\boldsymbol{e}_{0i} = \theta_i\,, \tag{34}$$

where '$\cdot$' denotes the scalar product of vectors. Therefore, in the foregoing we frequently use symbols $\boldsymbol{\theta}$ and $\boldsymbol{\vartheta}$ interchangeably, whenever there is no danger of confusion.

Interestingly enough one can construct a direct representation of the orthogonal rotation tensor $\boldsymbol{\Lambda}$ via vector $\boldsymbol{\theta}$, hence, by the abuse of the language, $\boldsymbol{\theta}$ is referred to as the *rotation vector*. This construction can be carried out according to Fig. 3 (see [28]) to get

$$\boldsymbol{\Lambda} = \cos\theta[\boldsymbol{I} - \boldsymbol{n}\otimes\boldsymbol{n}] + \sin\theta[\boldsymbol{n}\times\boldsymbol{I}] + [\boldsymbol{n}\otimes\boldsymbol{n}]\,, \tag{35}$$

where $\theta = \|\boldsymbol{\theta}\|$ is the magnitude of the rotation vector and $\boldsymbol{n} = \boldsymbol{\theta}/\theta$ is a unit vector along the rotation axis.

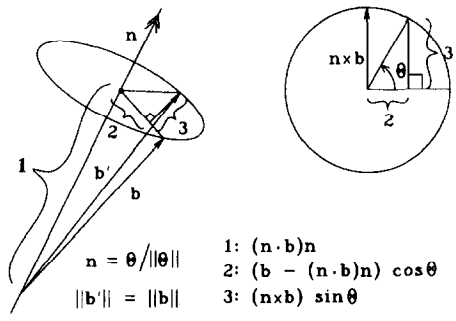

Fig. 3. Finite rotation of a vector.

The last expression can also be written in the form similar to the one in (14) given for the exponential mapping

$$\begin{aligned}\boldsymbol{\Lambda} &= \cos\theta \boldsymbol{I} + \frac{\sin\theta}{\theta}\boldsymbol{\Theta} + \frac{1-\cos\theta}{\theta^2}\boldsymbol{\theta}\otimes\boldsymbol{\theta} \\ &= \exp[\boldsymbol{\Theta}]\,, \end{aligned} \tag{36}$$

where $\boldsymbol{\Theta}$ is the skew-symmetric tensor for which $\boldsymbol{\theta}$ is the axial vector, i.e. $\boldsymbol{\Theta}\boldsymbol{b} = \boldsymbol{\theta}\times\boldsymbol{b}$; $\forall\, \boldsymbol{b}\in\mathbb{R}^3$.

We conclude that $\boldsymbol{\Theta}$ represents infinitesimal rotation corresponding to a finite rotation $\boldsymbol{\Lambda}$, and that $\boldsymbol{\Theta}$ is an element of the tangent space $T_1\mathrm{SO}(3)$.

REMARK 2. Another way to derive the exponential mapping formula is to use the definition of the exponential of a matrix (see e.g. [29])

$$\boldsymbol{\Lambda} := \sum_{k=0}^{\infty}\frac{1}{k!}\boldsymbol{\Theta}^k\,. \tag{37}$$

As shown by Argyris [6], by exploiting a certain number of identities based on the skew-symmetry of $\boldsymbol{\Theta}$, the last expression can be written as

$$\boldsymbol{\Lambda} = \boldsymbol{I} + \frac{\sin\theta}{\theta}\boldsymbol{\Theta} + \frac{1-\cos\theta}{\theta^2}\boldsymbol{\Theta}\boldsymbol{\Theta}\,, \tag{38}$$

which is an alternative form of the exponential mapping formula. However, by using the vector identity that $\boldsymbol{\theta}\times(\boldsymbol{\theta}\times\boldsymbol{b}) = (\boldsymbol{\theta}\otimes\boldsymbol{\theta} - \theta^2\boldsymbol{I})\boldsymbol{b}$; $\forall\,\boldsymbol{b}\in\mathbb{R}^3$,we can easily show that two forms of the exponential mapping are equivalent. □

There are numerous advantages to using rotation vector $\boldsymbol{\theta}$ as the primary variable, possibly the most important one being that the configuration space becomes linear

$$\mathscr{C} := \{(\boldsymbol{\chi}, \boldsymbol{\theta})\colon [0, L]\times[0, T]\mapsto\mathbb{R}^3\times\mathbb{R}^3\}\,. \tag{39}$$

3.3. Angular velocity parameters

Of special interest in this section is to establish the relationship between the rotation vector parameterization and the intrinsic parameterization of finite rotation discussed previously. To that end, we note that given two lines in the tangent space $T_1\mathrm{SO}(3)$, defined by $(t\boldsymbol{\Psi})$ and $(t\hat{\boldsymbol{\Theta}})$, we can construct a one parameter subgroup in two manners as

$$\exp[\hat{\boldsymbol{\Theta}} + t\dot{\hat{\boldsymbol{\Theta}}}] = \exp[\hat{\boldsymbol{\Theta}}]\exp[t\boldsymbol{\Psi}]\,; \qquad \hat{\boldsymbol{\Theta}}\boldsymbol{b} = \boldsymbol{\vartheta}\times\boldsymbol{b}\,. \tag{40}$$

Graphic illustration of these constructions is given in Fig. 4.

Using the standard result (see e.g. [29]) that $[\exp(\boldsymbol{\Theta})]^{-1} = \exp(-\boldsymbol{\Theta})$, the last expression can be rewritten as

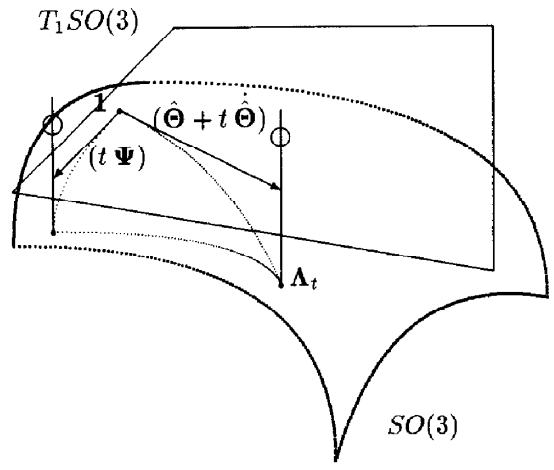

Fig. 4. Finite rotation decomposition in material representation.

$$\exp[t\boldsymbol{\Psi}] = \exp[-\hat{\boldsymbol{\Theta}}]\exp[\hat{\boldsymbol{\Theta}} + t\dot{\hat{\boldsymbol{\Theta}}}]\,. \tag{41}$$

Taking the time derivative of the expression above, and making use of the Lie bracket identities (see e.g. [30, p. 105]), we can obtain the following result (see [15])

$$\begin{aligned} &\boldsymbol{\psi} = \boldsymbol{T}^{\mathrm{T}}(\boldsymbol{\vartheta})\dot{\boldsymbol{\vartheta}}\,, \\ &\boldsymbol{T}(\boldsymbol{\vartheta}) = \frac{\sin\vartheta}{\vartheta}\boldsymbol{I} + \frac{1-\cos\vartheta}{\vartheta^2}\hat{\boldsymbol{\Theta}} + \frac{\vartheta - \sin\vartheta}{\vartheta^3}\boldsymbol{\vartheta}\otimes\boldsymbol{\vartheta}\,. \end{aligned} \tag{42}$$

We note in passing that expression in (42) above makes sense geometrically, since both $\boldsymbol{\Psi}$ and $\hat{\boldsymbol{\Theta}}$ are the elements of tangent space T_1SO(3) (see Fig. 4).

It is worthy of further attention that tensors $\boldsymbol{T}$ and $\boldsymbol{\Lambda}$ are linear combinations of the same elementary tensors; Moreover, it can be shown (see [15]) that they share the same eigenvectors, and hence they commute.

By the direct multiplication, we can also verify another interesting property of tensors $\boldsymbol{T}$ and $\boldsymbol{\Lambda}$ in that

$$\boldsymbol{T}^{\mathrm{T}}\boldsymbol{\Lambda} = \boldsymbol{T}\,. \tag{43}$$

The last result can be exploited to obtain that

$$\begin{aligned} \boldsymbol{w} &= \boldsymbol{\Lambda}\boldsymbol{\psi} \\ &= \boldsymbol{T}^{\mathrm{T}}\boldsymbol{\Lambda}\boldsymbol{I}^{-1}\dot{\boldsymbol{\theta}} \\ &= \boldsymbol{T}\dot{\boldsymbol{\theta}}\,. \end{aligned} \tag{44}$$

The commutative diagram in Fig. 5 summarizes the different possibilities to parameterize the angular velocities and their mutual relationships.[3]

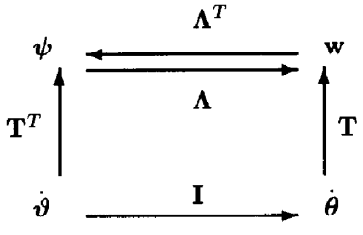

Fig. 5. Commutative diagram of time derivative of finite rotations parameters.

[3] The same diagram applies to admissible variations of rotation parameters, as well as their increments.

3.4. Singularity in rotation vector parameterization

As shown by Stuelpnagel [19], not a single 3-parameter representation of finite rotation is singularity-free in a global sense. For the particular choice of rotation vector parameters, this can be shown in the most elegant manner by using its principal axis representation.

Spectral decomposition of tensor $\boldsymbol{\Lambda}$ can be written as

$$\boldsymbol{\Lambda} = \lambda_1 \boldsymbol{n} \otimes \boldsymbol{n} + \lambda_2 \boldsymbol{n}_2 \otimes \boldsymbol{n}^2 + \lambda_3 \boldsymbol{n}_3 \otimes \boldsymbol{n}^3 , \tag{45}$$

where λ_i are the principal values, given as

$$\lambda_1 = 1 ; \qquad \lambda_2 = \cos\theta + i \sin\theta ; \qquad \lambda_3 = \cos\theta - i \sin\theta , \tag{46}$$

whereas $\boldsymbol{n}_i$ and $\boldsymbol{n}^i$ are, respectively, the corresponding principal vector and co-vector.[4] In particular, the first principal vector and co-vector are the same as the normalized rotation vector

$$\boldsymbol{n}_1 \equiv \boldsymbol{n}^1 \equiv \boldsymbol{n} = \begin{pmatrix} \theta_1/\theta \\ \theta_2/\theta \\ \theta_3/\theta \end{pmatrix} = \begin{pmatrix} n_1 \\ n_2 \\ n_3 \end{pmatrix} \tag{47}$$

and the remaining eigenvector pairs are given as

$$\boldsymbol{n}_2 = \begin{pmatrix} 1 \\ \dfrac{-n_1 n_2 - i n_3}{n_2^2 + n_3^2} \\ \dfrac{-n_1 n_3 + i n_2}{n_2^2 + n_3^2} \end{pmatrix} ; \qquad \boldsymbol{n}_3 = \begin{pmatrix} 1 \\ \dfrac{-n_1 n_2 + i n_3}{n_2^2 + n_3^2} \\ \dfrac{-n_1 n_3 - i n_2}{n_2^2 + n_3^2} \end{pmatrix} ; \qquad \boldsymbol{n}^2 = \begin{pmatrix} \dfrac{n_2^2 + n_3^2}{2} \\ \dfrac{-n_1 n_2 + i n_3}{2} \\ \dfrac{-n_1 n_3 - i n_2}{2} \end{pmatrix} ;$$

$$\boldsymbol{n}^3 = \begin{pmatrix} \dfrac{n_2^2 + n_3^2}{2} \\ \dfrac{-n_1 n_2 - i n_3}{2} \\ \dfrac{-n_1 n_3 + i n_2}{2} \end{pmatrix} . \tag{48}$$

REMARK 3. It is interesting to note that the corresponding skew-symmetric tensor $\boldsymbol{\Theta}$ also shares the same principal vector and co-vectors, and that the corresponding eigenvalues are given as

$$\lambda_{\theta_1} = 0 ; \qquad \lambda_{\theta_2} = \mathrm{i}\theta ; \qquad \lambda_{\theta_3} = -\mathrm{i}\theta . \tag{49}$$

Therefore, in the space of principal directions the exponential mapping is reduced to the exponentiation of the principal values of $\boldsymbol{\Theta}$ in order to obtain the principal values of $\boldsymbol{\Lambda}$, i.e. $\lambda_i = \exp(\lambda_{\theta_i})$. □

It is easy to verify (see [15]) that the spectral decomposition of tensor $\boldsymbol{T}$ can be computed by employing the same principal vectors and co-vectors

$$\boldsymbol{T} = \lambda_{T_1} \boldsymbol{n} \otimes \boldsymbol{n} + \lambda_{T_2} \boldsymbol{n}_2 \otimes \boldsymbol{n}^2 + \lambda_{T_3} \boldsymbol{n}_3 \otimes \boldsymbol{n}^3 \tag{50}$$

and that its principal values are given as

$$\lambda_{T_1} = 1 ; \qquad \lambda_{T_2} = \frac{\sin\theta}{\theta} + i \frac{1 - \cos\theta}{\theta} ; \qquad \lambda_{T_2} = \frac{\sin\theta}{\theta} - i \frac{1 - \cos\theta}{\theta} . \tag{51}$$

[4] In the terminology of linear algebra (see e.g. [31, p. 370]) the principal vectors and co-vectors correspond to the right and the left eigenvectors, respectively.

Principal axis representation of tensor $\boldsymbol{T}$ simplifies the computation of its determinant to

$$\begin{aligned}\det(\boldsymbol{T}) &= \lambda_{T_1}\lambda_{T_2}\lambda_{T_3} \\ &= \frac{2(1-\cos\theta)}{\theta^2}.\end{aligned} \tag{52}$$

The last result reveals that the mapping between the three-parameter rotation vector parameterization and the intrinsic, nine-parameter representation of finite rotation ceases to be a bijection for rotations $\theta = 2k\pi$, where k is an integer, which thus reiterates the result of Stuelpnagel [19].

4. Proposed finite rotation parameterization

4.1. Incremental rotation vector

Having concluded that the rotation vector parameterization can not in general be retained globally, we turn to examining its utility within the framework of an incremental procedure used in the solution of nonlinear problems. If the evolution of configuration space variables is obtained by a time-stepping scheme, the time interval of interest is partitioned into a number of time steps: $0 < t_1 < t_2 < \cdots < t_n < t_{n+1} < \cdots < T$. At a typical time t_n, the values of translation and rotation motion components are denoted as

$$\boldsymbol{\chi}_n = \boldsymbol{\chi}(t_n); \qquad \boldsymbol{\Lambda}_n = \boldsymbol{\Lambda}(t_n). \tag{53}$$

We consider the case when one-step schemes are used to advance the evolution of the state variables over a typical time increment, so that their values at time t_{n+1} are computed solely on the basis of the corresponding values at time t_n. For displacement vector update we have

$$\boldsymbol{\chi}_{n+1} = \boldsymbol{\chi}_n + \boldsymbol{u}_{n+1}, \tag{54}$$

where $\boldsymbol{u}_{n+1}$ are incremental displacements.

According to the discussion in Section 2, for rotation update we need to choose between two possibilities corresponding to the spatial and material representations. If we denote the *spatial* incremental rotation vector $\boldsymbol{\theta}_{n+1}$ and the *material* incremental rotation vector $\boldsymbol{\vartheta}_{n+1}$, with the corresponding skew-symmetric tensors $\boldsymbol{\Theta}_{n+1}$ and $\hat{\boldsymbol{\Theta}}_{n+1}$, the rotation update can be carried out as

$$\begin{aligned}\boldsymbol{\Lambda}_{n+1} &= \tilde{\boldsymbol{\Lambda}}(\boldsymbol{\theta}_{n+1})\boldsymbol{\Lambda}_n \\ &= \boldsymbol{\Lambda}_n\tilde{\boldsymbol{\Lambda}}(\boldsymbol{\vartheta}_{n+1}),\end{aligned} \tag{55}$$

where $\tilde{\boldsymbol{\Lambda}}(\boldsymbol{\theta}_{n+1}) := \exp(\boldsymbol{\Theta}_{n+1})$ is given by the exponential mapping formula in (14). By considering that $\boldsymbol{\Lambda}_n$ is an orthogonal tensor, from (55) above we can obtain that

$$\begin{aligned}\tilde{\boldsymbol{\Lambda}}(\boldsymbol{\theta}_{n+1}) &= \boldsymbol{\Lambda}_n\tilde{\boldsymbol{\Lambda}}(\boldsymbol{\vartheta}_{n+1})\boldsymbol{\Lambda}_n^{\mathrm{T}} \\ \tilde{\boldsymbol{\Lambda}}(\boldsymbol{\vartheta}_{n+1}) &= \boldsymbol{\Lambda}_n^{\mathrm{T}}\tilde{\boldsymbol{\Lambda}}(\boldsymbol{\theta}_{n+1})\boldsymbol{\Lambda}_n.\end{aligned} \tag{56}$$

Furthermore, by taking into account (see Remark 3) that a skew-symmetric tensor and the corresponding orthogonal tensor obtained by its exponentiation share the same eigenvectors, from (56) above it follows that

$$\begin{aligned}\boldsymbol{\Theta}_{n+1} &= \boldsymbol{\Lambda}_n\hat{\boldsymbol{\Theta}}_{n+1}\boldsymbol{\Lambda}_n^{\mathrm{T}} \\ \hat{\boldsymbol{\Theta}}_{n+1} &= \boldsymbol{\Lambda}_n^{\mathrm{T}}\boldsymbol{\Theta}_{n+1}\boldsymbol{\Lambda}_n.\end{aligned} \tag{57}$$

The last result can also be written in terms of the spatial and material incremental rotation vectors

$$\begin{aligned}\boldsymbol{\theta}_{n+1} &= \boldsymbol{\Lambda}_n\boldsymbol{\vartheta}_{n+1} \\ \boldsymbol{\vartheta}_{n+1} &= \boldsymbol{\Lambda}_n^{\mathrm{T}}\boldsymbol{\theta}_{n+1}.\end{aligned} \tag{58}$$

In sharp contrast with the total rotation vector in (33), the spatial and material representations of the incremental

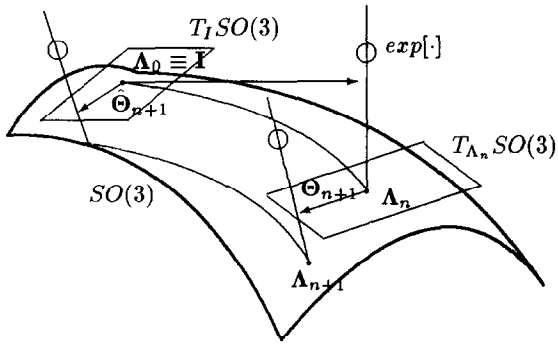

Fig. 6. Incremental rotation vector in spatial and material representations.

rotation vectors are not the same. The graphical representation of these relations is given in Fig. 6. It is important to note that $\boldsymbol{\Theta}_{n+1}$ and $\hat{\boldsymbol{\Theta}}_{n+1}$ belong, respectively, to the tangent spaces $T_{\Lambda_n}\mathrm{SO}(3)$ and $T_I\mathrm{SO}(3)$.

4.2. Integral form of balance equations

In this section we briefly examine the consequences to making this choice of rotation parameters on the integral form of balance equations. We first note that the axial and shear strains at time t_{n+1} can now be written as

$$\boldsymbol{\epsilon}_{n+1} = \boldsymbol{u}'_{n+1} + [\boldsymbol{I} - \tilde{\boldsymbol{\Lambda}}(\boldsymbol{\theta}_{n+1})]\boldsymbol{\chi}'_n + \tilde{\boldsymbol{\Lambda}}(\boldsymbol{\theta}_{n+1})\boldsymbol{\epsilon}_n , \tag{59}$$

whereas the bending strains can be written as

$$\boldsymbol{\kappa}_{n+1} = \tilde{\boldsymbol{T}}(\boldsymbol{\theta}_{n+1})\boldsymbol{\theta}'_{n+1} + \tilde{\boldsymbol{\Lambda}}(\boldsymbol{\theta}_{n+1})\boldsymbol{\kappa}_n , \tag{60}$$

where their values at time t_n, $\boldsymbol{\epsilon}_n$ and $\boldsymbol{\kappa}_n$, are assumed to be known. The bending strains are composed of two terms. The first one is formally equivalent to the angular velocity expression in (44) but with the incremental rotation vector and space-coordinate derivative replacing, respectively, the total rotation vector and time-derivative. The last term, on the other hand, can be recognized as a parallel transport (see e.g. [30]) of the bending strain $\boldsymbol{\kappa}_n$ on SO(3) manifold. The same term is also found in the construction of the axial and shear strains.

The energy-conjugate stress resultants and couples can now be obtained as

$$\boldsymbol{n}_{n+1} = \tilde{\boldsymbol{\Lambda}}(\boldsymbol{\theta}_{n+1})\boldsymbol{\Lambda}_n \boldsymbol{C} \boldsymbol{\Lambda}_n^{\mathrm{T}} \tilde{\boldsymbol{\Lambda}}^{\mathrm{T}}(\boldsymbol{\theta}_{n+1})\boldsymbol{\epsilon}_{n+1} \tag{61}$$

and

$$\boldsymbol{m}_{n+1} = \tilde{\boldsymbol{\Lambda}}(\boldsymbol{\theta}_{n+1})\boldsymbol{\Lambda}_n \boldsymbol{D} \boldsymbol{\Lambda}_n^{\mathrm{T}} \tilde{\boldsymbol{\Lambda}}^{\mathrm{T}}(\boldsymbol{\theta}_{n+1})\boldsymbol{\kappa}_{n+1} \tag{62}$$

Furthermore, due to the multiplicative rotation decomposition in (55), $\boldsymbol{\Lambda}_n$ drops out from the computation of the strain rates by using the Lie derivative formalism, so that the corresponding expression in (27) can be rewritten as

$$L_w[(\bullet)] = \tilde{\boldsymbol{\Lambda}}(\boldsymbol{\theta}_{n+1}) \frac{\mathrm{d}}{\mathrm{d}t}\bigg|_{t=1} [\tilde{\boldsymbol{\Lambda}}(\boldsymbol{\theta}_{n+1,t})(\bullet)_t] . \tag{63}$$

In particular, the strain rates for the axial and shear strain can be computed as

$$L_w[\boldsymbol{\epsilon}_{n+1}] = \dot{\boldsymbol{u}}_{n+1} + \boldsymbol{\chi}'_{n+1} \times \tilde{\boldsymbol{T}}(\boldsymbol{\theta}_{n+1})\dot{\boldsymbol{\theta}}_{n+1} \tag{64}$$

and the strain rate for the bending strain is

$$L_w[\boldsymbol{\kappa}_{n+1}] = \tilde{\boldsymbol{T}}(\boldsymbol{\theta}_{n+1})\dot{\boldsymbol{\theta}}'_{n+1} + \tilde{\boldsymbol{R}}(\boldsymbol{\theta}_{n+1})\dot{\boldsymbol{\theta}}_{n+1} + \tilde{\boldsymbol{T}}(\boldsymbol{\theta}_{n+1})\boldsymbol{\theta}'_{n+1} \times \tilde{\boldsymbol{T}}(\boldsymbol{\theta})\dot{\boldsymbol{\theta}}_{n+1} , \tag{65}$$

where

$$\tilde{\boldsymbol{R}}(\boldsymbol{\theta}_{n+1}) = c_1[\boldsymbol{\theta}'_{n+1} \otimes \boldsymbol{\theta}_{n+1}] + c_2[(\boldsymbol{\theta}_{n+1} \times \boldsymbol{\theta}'_{n+1}) \otimes \boldsymbol{\theta}_{n+1}] + c_3(\boldsymbol{\theta}_{n+1} \cdot \boldsymbol{\theta}'_{n+1})[\boldsymbol{\theta}_{n+1} \otimes \boldsymbol{\theta}_{n+1}] - c_4[\boldsymbol{\Theta}'_{n+1}] + c_5(\boldsymbol{\theta}_{n+1} \cdot \boldsymbol{\theta}'_{n+1})[\boldsymbol{I}] + c_5[\boldsymbol{\theta}_{n+1} \otimes \boldsymbol{\theta}'_{n+1}], \tag{66}$$

with

$$c_1 = \frac{\theta_{n+1}\cos\theta_{n+1} - \sin\theta_{n+1}}{\theta^3_{n+1}}, \qquad c_2 = \frac{\theta_{n+1}\sin\theta_{n+1} + 2\cos\theta_{n+1} - 2}{\theta^4_{n+1}},$$
$$c_3 = \frac{3\sin\theta_{n+1} - 2\theta_{n+1} - \theta_{n+1}\cos\theta_{n+1}}{\theta^5_{n+1}}, \qquad c_4 = \frac{1 - \cos\theta_{n+1}}{\theta^2_{n+1}}, \tag{67}$$
$$c_5 = \frac{\theta_{n+1} - \sin\theta_{n+1}}{\theta^3_{n+1}}.$$

Using these results, the integral form of the momentum balance equations can be obtained as a function of incremental displacement and incremental rotation vector only,

$$G(\boldsymbol{u}_{n+1}, \boldsymbol{\theta}_{n+1}, \dot{\boldsymbol{u}}_{n+1}, \dot{\boldsymbol{\theta}}_{n+1}) = 0. \tag{68}$$

In other words, in each increment, the beam configuration space is formally presented as a linear space

$$\mathscr{C}_{n+1} := \{(\boldsymbol{u}_{n+1}, \boldsymbol{\theta}_{n+1}) : [0, L] \times [t_n, t_{n+1}] \mapsto \mathbb{R}^3 \times \mathbb{R}^3\}. \tag{69}$$

We note in passing that using the rotation vector parameterization in each increment, we are not likely to experience the problem associated with the presence of singularity at multiples of 2π. Such large rotation increments are anyway precluded by a limited size of the ball of convergence of most iterative procedures.

4.3. Iterative rotation updates

The final values of the state variables in each increment are established by an iterative procedure which ensures the satisfaction of the integral form of the balance equations. Details pertinent to the iterative updates of the chosen rotation parameters are discussed in this section. To that end, let superscript '(i)' denote the iteration counter. At each iteration, the incremental displacement update is performed in the standard, additive fashion as

$$\boldsymbol{u}^{(i+1)}_{n+1} = \boldsymbol{u}^{(i)}_{n+1} + \Delta\boldsymbol{u}^{(i)}_{n+1}, \tag{70}$$

where $\Delta\boldsymbol{u}^{(i)}_{n+1}$ is the (i)th iteration contribution to the incremental displacement field.

The iterative update of finite rotations is more involved in that not only do we have to choose between spatial and material representations, but also between different iterative rotation parameters. To elaborate upon the latter, we first consider the material form of the iterative rotation parameters and the kind of the rotation update where we make use of the exponential mapping at each iteration to get

$$\boldsymbol{\Lambda}^{(i+1)}_{n+1} = \boldsymbol{\Lambda}^{(i)}_{n+1}\tilde{\boldsymbol{\Lambda}}(\Delta\boldsymbol{\psi}^{(i)}_{n+1}), \tag{71}$$

where $\Delta\boldsymbol{\psi}^{(i)}_{n+1}$ is material form of the iterative rotation vector. The same value of the total rotation, $\boldsymbol{\Lambda}^{(i+1)}_{n+1}$, can be obtained by making use of the material form of the incremental rotation vector $\boldsymbol{\vartheta}^{(i)}_{n+1}$ and its iterative increment $\Delta\boldsymbol{\vartheta}^{(i)}_{n+1}$. Since both are the elements of a linear space, $T_I\mathrm{SO}(3)$, they can directly be superposed to get

$$\boldsymbol{\Lambda}^{(i+1)}_{n+1} = \boldsymbol{\Lambda}_n\tilde{\boldsymbol{\Lambda}}(\boldsymbol{\vartheta}^{(i)}_{n+1} + \Delta\boldsymbol{\vartheta}^{(i)}_{n+1}). \tag{72}$$

From the last two expressions and the incremental rotation vector definition in (55), we can obtain

$$\tilde{\boldsymbol{\Lambda}}(\epsilon\,\Delta\boldsymbol{\psi}^{(i)}_{n+1}) = \tilde{\boldsymbol{\Lambda}}(-\boldsymbol{\vartheta}^{(i)}_{n+1})\tilde{\boldsymbol{\Lambda}}(\boldsymbol{\vartheta}^{(i)}_{n+1} + \epsilon\,\Delta\boldsymbol{\vartheta}^{(i)}_{n+1}), \tag{73}$$

which, by the analogy with the procedure described in the previous section for angular velocity computation, further leads to

$$\Delta\boldsymbol{\psi}^{(i)}_{n+1} = \tilde{\boldsymbol{T}}^{\mathrm{T}}(\boldsymbol{\vartheta}^{(i)}_{n+1})\,\Delta\boldsymbol{\vartheta}^{(i)}_{n+1}. \tag{74}$$

If the spatial representation of the iterative rotation parameters is used, we can carry out the rotation updates as

$$\begin{aligned}\boldsymbol{\Lambda}_{n+1}^{(i+1)} &= \tilde{\boldsymbol{\Lambda}}(\boldsymbol{\theta}_{n+1}^{(i)} + \Delta\boldsymbol{\theta}_{n+1}^{(i)})\boldsymbol{\Lambda}_n \\ &= \tilde{\boldsymbol{\Lambda}}(\Delta\boldsymbol{w}_{n+1}^{(i)})\boldsymbol{\Lambda}_{n+1}^{(i)} .\end{aligned} \tag{75}$$

The graphic illustration of these two iterative rotation updates is presented in Fig. 7.

Contrary to the material representations of incremental rotation updates, the mutual relationship between the two spatial representations of iterative rotation parameters is no longer analogous to the angular velocity relation established in (44). In order to derive the relationship of this kind we use

$$\Delta\boldsymbol{w}_{n+1}^{(i)} = \boldsymbol{\Lambda}_{n+1}^{(i)}\,\Delta\boldsymbol{\psi}_{n+1}^{(i)} ; \qquad \Delta\boldsymbol{\theta}_{n+1}^{(i)} = \boldsymbol{\Lambda}_n\,\Delta\boldsymbol{\vartheta}_{n+1}^{(i)} , \tag{76}$$

which, along with the relationships in (55) and (74) further leads to

$$\begin{aligned}\Delta\boldsymbol{w}_{n+1}^{(i)} &= \boldsymbol{\Lambda}_{n+1}^{(i)}\tilde{\boldsymbol{T}}^{\mathrm{T}}(\boldsymbol{\vartheta}_{n+1}^{(i)})\boldsymbol{\Lambda}_n^{\mathrm{T}}\,\Delta\boldsymbol{\theta}_{n+1}^{(i)} \\ &= \tilde{\boldsymbol{\Lambda}}(\boldsymbol{\theta}_{n+1}^{(i)})\boldsymbol{\Lambda}_n\tilde{\boldsymbol{T}}(\boldsymbol{\vartheta}_{n+1}^{(i)})\boldsymbol{\Lambda}_n^{\mathrm{T}}\,\Delta\boldsymbol{\theta}_{n+1}^{(i)} .\end{aligned} \tag{77}$$

Furthermore, if we recall (see Section 3) that tensors $\boldsymbol{T}$ and $\boldsymbol{\Lambda}$ share the same eigenvectors, from (56) we can obtain

$$\begin{aligned}\tilde{\boldsymbol{T}}(\boldsymbol{\theta}_{n+1}^{(i)}) &= \boldsymbol{\Lambda}_n\tilde{\boldsymbol{T}}(\boldsymbol{\vartheta}_{n+1}^{(i)})\boldsymbol{\Lambda}_n^{\mathrm{T}} \\ \tilde{\boldsymbol{T}}(\boldsymbol{\vartheta}_{n+1}^{(i)}) &= \boldsymbol{\Lambda}_n^{\mathrm{T}}\tilde{\boldsymbol{T}}(\boldsymbol{\vartheta}_{n+1}^{(i)})\boldsymbol{\Lambda}_n .\end{aligned} \tag{78}$$

Replacing the last result into (77), we finally obtain

$$\begin{aligned}\Delta\boldsymbol{w}_{n+1}^{(i)} &= \tilde{\boldsymbol{\Lambda}}(\boldsymbol{\theta}_{n+1}^{(i)})\tilde{\boldsymbol{T}}^{\mathrm{T}}(\boldsymbol{\theta}_{n+1}^{(i)})\,\Delta\boldsymbol{\theta}_{n+1}^{(i)} \\ &= \tilde{\boldsymbol{T}}(\boldsymbol{\theta}_{n+1}^{(i)})\,\Delta\boldsymbol{\theta}_{n+1}^{(i)} .\end{aligned} \tag{79}$$

The results obtained in this section on the mutual relationship of iterative rotation parameters in spatial and material representation can all be summarized in Fig. 8.

4.4. Dynamics and implicit time-stepping schemes

The preceding discussion presents the full account for handling finite rotation updates, and related computational issues in the framework of static analysis. In dynamics, we also need to elaborate upon the computation of linear and angular momenta, which, according to the corresponding expressions in (25) and (26), requires that the angular velocities and accelerations at time t_{n+1} be provided.

In this section we focus upon the pertinent implementation details of one-step schemes used for that purpose. In that respect, with the treatment of displacement degrees of freedom being quite standard, it only remains to address the issues pertinent to the time-stepping scheme for the rotational degrees of freedom. Therefore, we

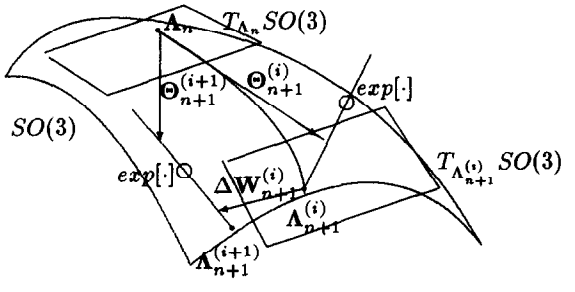

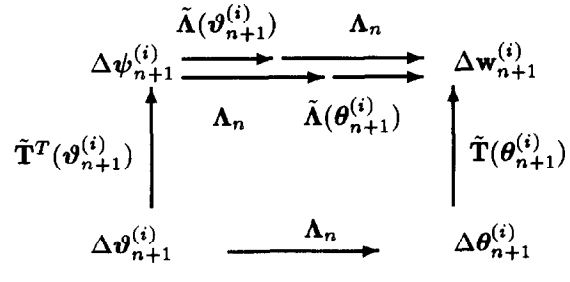

Fig. 7. Iterative updates of rotation in spatial representation.

Fig. 8. Commutative diagram for finite rotation iterative parameters.

assume that the corresponding values of angular velocities and accelerations are known at time t_n in either the spatial representation, with $\boldsymbol{w}_n = \boldsymbol{w}(t_n)$, $\boldsymbol{\alpha}_n = \dot{\boldsymbol{w}}(t_n)$, or the material one, with $\boldsymbol{\psi}_n = \boldsymbol{\psi}(t_n)$, $\boldsymbol{\iota}_n = \dot{\boldsymbol{\psi}}(t_n)$.

As first noted in [22] and [12], standard implementation of a typical one-step scheme, can directly be used only if the material representation of rotations is used. For example, with the Newmark scheme (see [32]) we can construct the approximations for angular velocity and acceleration according to

$$\boldsymbol{\psi}_{n+1} = \frac{\gamma}{\beta h}\boldsymbol{\vartheta}_{n+1} + \frac{\beta-\gamma}{\beta}\boldsymbol{\psi}_n + \frac{(\beta-0.5\gamma)h}{\beta}\boldsymbol{\iota}_n \tag{80}$$

and

$$\boldsymbol{\iota}_{n+1} = \frac{1}{\beta h^2}\boldsymbol{\vartheta}_{n+1} - \frac{1}{\beta h}\boldsymbol{\psi}_n - \frac{0.5-\beta}{\beta}\boldsymbol{\iota}_n\,, \tag{81}$$

where β and γ are the Newmark coefficients. Only these approximations make sense geometrically, since all the objects are the elements of the same tangent (linear) space, $T_I SO(3)$. In that respect, direct application of these approximations in the spatial representation would not be valid.

However, as noted recently by Ibrahimbegovic and Al Mikdad [33], we can devise the Newmark approximation valid for the spatial representation of the incremental rotation vector.[5] Namely, by pre-multiplying by $\boldsymbol{\Lambda}_n$ the two last expressions, and exploiting the results in (58), (20) and (24) to express, respectively, incremental rotation vector, angular velocity and angular acceleration in spatial representation we obtain

$$\boldsymbol{\Lambda}_n\boldsymbol{\psi}_{n+1} = \frac{\gamma}{\beta h}\boldsymbol{\theta}_{n+1} + \tilde{\boldsymbol{w}}_{n+1} \tag{82}$$

$$\boldsymbol{\Lambda}_n\boldsymbol{\iota}_{n+1} = \frac{1}{\beta h^2}\boldsymbol{\theta}_{n+1} + \tilde{\boldsymbol{\alpha}}_{n+1}\,, \tag{83}$$

where $\tilde{\boldsymbol{w}}_{n+1}$ and $\tilde{\boldsymbol{\alpha}}_{n+1}$ are given as

$$\tilde{\boldsymbol{w}}_{n+1} = \frac{\beta-\gamma}{\beta}\boldsymbol{w}_n + \frac{\beta-0.5\gamma}{\beta}h\boldsymbol{\alpha}_n \tag{84}$$

$$\tilde{\boldsymbol{\alpha}}_{n+1} = -\frac{1}{\beta h}\boldsymbol{w}_n - \frac{0.5-\beta}{\beta}\boldsymbol{\alpha}_n\,. \tag{85}$$

We note that all the objects appearing on the left-hand side of these last four equations are elements of the tangent space $T_{\Lambda_n}SO(3)$, and that it makes sense geometrically to combine them, see Fig. 9.

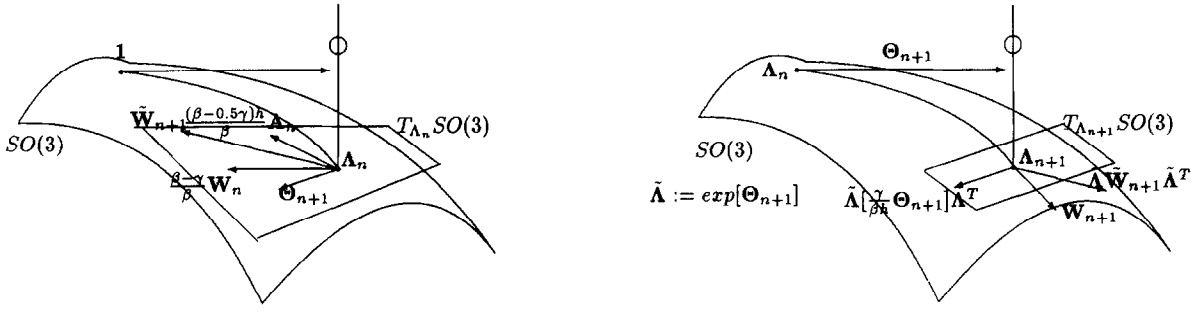

Fig. 9. Spatial form of Newmark approximation for angular velocity: basic ingredients.

Fig. 10. Spatial form of Newmark approximation for angular velocity: parallel transport.

[5] The main interest of such an approximation is in rather sparse structure of the tangent operator (see [33], for details).

Hence, by the parallel transport (see e.g. [30]) of these objects to tangent space $T_{\Lambda_{n+1}}\mathrm{SO}(3)$ (see Fig. 10), we obtain the spatial form of the Newmark approximations for finite rotations as

$$\boldsymbol{w}_{n+1} = \tilde{\boldsymbol{\Lambda}}(\boldsymbol{\theta}_{n+1})\left[\frac{\gamma}{\beta h}\boldsymbol{\theta}_{n+1} + \tilde{\boldsymbol{w}}_{n+1}\right] \tag{86}$$

and

$$\boldsymbol{\alpha}_{n+1} = \tilde{\boldsymbol{\Lambda}}(\boldsymbol{\theta}_{n+1})\left[\frac{1}{\beta h^2}\boldsymbol{\theta}_{n+1} + \tilde{\boldsymbol{\alpha}}_{n+1}\right]. \tag{87}$$

It is apparent that the incremental rotation vector also plays a key role in updating the values of angular velocities and accelerations.

5. Numerical examples

In this section we present several numerical examples to illustrate the performance of the proposed rotation parameterization. All the computations are performed with an enhanced version of the computer program *FEAP*, developed by Prof. R.L. Taylor at UC Berkeley (see [34]). We choose the simplest finite element approximations of the reference geometry, based on 2-node beam elements with linear shape functions. Furthermore, the isoparametric approximations (see e.g. [34]) are employed for the state variables, their variations and increments.

5.1. Roll-up of a beam under moment and perturbation force

We first examine the test problem (see e.g. [11]) of the pure bending of a cantilever beam under concentrated moment applied at its free end (see Fig. 11). The selected properties of the cantilever are: length $l = 10$, axial stiffness $EA = 10^4$, shear stiffness $GA = 10^4$, bending stiffness $EI = 10^2$ and torsional stiffness $GJ = 10^2$.

In the case when the perturbation force $F = 0$, the only non-trivial deformation component is the flexural one. Moreover, according to the classical Euler formula, this bending deformation is constant along the beam. It thus follows that the beam deformed shape must be a part of a circle, and that the analytic solution for the free-end displacement components can be obtained as

$$\begin{aligned} \theta &= \frac{Ml}{EI} \\ u_1 &= l - \frac{l}{\theta/2}\sin\frac{\theta}{2}\cos\theta\frac{\theta}{2} \\ u_2 &= \frac{l}{\theta/2}\left(\sin\frac{\theta}{2}\right)^2. \end{aligned} \tag{88}$$

The free-end displacements obtained by the analytic solution for the value of the bending moment $M = 2.5\pi$, are presented in Table 1. The corresponding numerical result, obtained by a mesh of 10 beam elements employing the incremental rotation vector, is also given in Table 1.

Similar results are finally obtained by the same number of 2-node beam elements of Simo and Vu-Quoc [11] with the *non-symmetric* tangent stiffness matrix, as well as the equivalent beam element obtained by

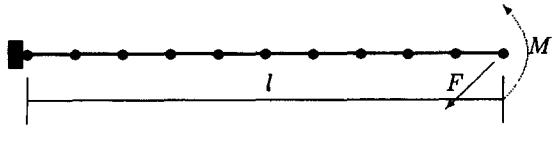

Fig. 11. Cantilever beam under end moment and perturbation force.

Table 1
Displacement components under end moment

Model	Disp. u_1	Disp. u_2	Disp. u_3
Incr. rotation vector	−0.994522	3.73019	0.
Λ—symm	−0.994522	3.73019	0.
Λ—non-symm	−0.994522	3.73019	0.
Analytic	−0.996837	3.72923	0.

symmetrizing the element stiffness matrix, as suggested by Simo [7]. These results are denoted, respectively, as Λ—symm and Λ—non-symm parameterizations.

We can see that the computed values of the displacements are very close to the analytic values, and that the present beam model is capable of representing the classical solution of Euler. (The solution for the rotation are identical to the analytic one.)

The convergence rate of the solution, as given in Table 2 for all the rotation parameterization utilized, is extremely good; We only need 2 iterations to converge. This exceptional performance is the consequence of a simple deformation pattern with all the deformations being constant along the beam.

In the second version of the same test we keep all the data the same as in the first version, except that we add a perturbation-type of force $F = 0.001$ perpendicular to the plane of the bending moment (see Fig. 7). The computed free-end displacement components, as given in Table 3, are very slightly perturbed with respect to the corresponding ones in Table 1. Moreover, the present parameterization leads to essentially the same values of the displacements as those computed with two Λ parameterization.

Two different forms of the tangent stiffness matrix used for the (intrinsic) Λ parameterization of finite rotations, employing the symmetric and non-symmetric tangent operators, quite naturally have no effect on the computed values for the displacements, since the residual vector computation remains the same. On the other hand, the rate of convergence is rather strongly influenced by the choice of the tangent stiffness, see Table 4.

The careful considerations of the consistent linearization issues pertinent to the proposed vector-like parameterization of finite rotations, once again result in the quadratic convergence rate of the iterative solution. On the other hand, a disappointingly slow rate of convergence of the Λ parameterization of large rotations ([6, 11]) is found when the tangent stiffness matrix is symmetrized (see [7]).

This loss of quadratic convergence properties of the symmetrized tangent stiffness is not quite surprising and

Table 2
Convergence rates under end moment

	Incr. rotation vector		Λ—symm		Λ—non-symm	
It.	Residual	Energy	Residual	Energy	Residual	Energy
0	7.854×10^{0}	6.169×10^{0}	7.854×10^{0}	6.169×10^{0}	7.854×10^{0}	6.169×10^{0}
1	3.374×10^{3}	1.841×10^{3}	3.374×10^{3}	1.841×10^{3}	3.374×10^{3}	1.841×10^{3}
2	1.468×10^{-11}	6.169×10^{-23}	1.189×10^{-11}	2.208×10^{-23}	1.570×10^{-11}	2.178×10^{-23}

Table 3
Displacement components under end moment and pert. force

Model	Disp. u_1	Disp. u_2	Disp. u_3
Incr. rotation vector	−0.994523	3.73019	0.003250
Λ—symm	−0.994523	3.73019	0.003122
Λ—non-symm	−0.994523	3.73019	0.003122

Table 4
Convergence rates under end moment and pert. force

	Incr. rotation vector		Λ—symm		Λ—non-symm	
It.	Residual	Energy	Residual	Energy	Residual	Energy
0	7.854×10^{0}	6.169×10^{0}	7.854×10^{0}	6.169×10^{0}	7.854×10^{0}	6.169×10^{0}
1	3.374×10^{3}	1.841×10^{3}	3.374×10^{3}	1.841×10^{3}	3.374×10^{3}	1.841×10^{3}
2	1.202×10^{-4}	2.519×10^{-9}	2.849×10^{-3}	1.246×10^{-6}	1.098×10^{-3}	4.184×10^{-8}
3	9.054×10^{-7}	1.392×10^{-16}	1.456×10^{-3}	2.039×10^{-7}	2.738×10^{-6}	9.463×10^{-16}
4	7.966×10^{-12}	2.038×10^{-27}	5.885×10^{-4}	3.495×10^{-8}	9.693×10^{-12}	3.498×10^{-27}
5			2.386×10^{-4}	5.988×10^{-9}		
6			9.872×10^{-5}	1.026×10^{-9}		
7			4.085×10^{-5}	1.759×10^{-10}		
8			1.691×10^{-5}	3.014×10^{-11}		
9			6.999×10^{-6}	5.166×10^{-12}		
			...			
30			6.873×10^{-12}	4.139×10^{-27}		

can be explained as the consequence of the non-conservative nature of the bending moment in the presence of the lateral motion of the beam produced by the out-of-plane perturbation force (see [6]). However, what we believe is a particularly disturbing finding is that performance of the symmetrized Λ-parameterization deteriorates so sharply, even for a fairly small perturbation from the ideal case.

5.2. Beam bent to a helical form

In this example we take the cantilever beam defined in the previous example (see Fig. 11), and subject it to an increased value of moment $M = 200\pi$ and the out-of-plane force $F = 50$.

It is important to note that very large rotation corresponding to free-end component of $\theta = 20\pi$, would result from this bending moment acting alone, and that the deformed shape would be a circular one, produced with a ten-fold roll-up of the beam. Hence, in order to ensure the sufficient accuracy of the computed displacement values, we use a finite element model composed of 100 beam elements employing the incremental rotation vector.

The simultaneous application of the moment and the force produces a helical deformed shape. A sequence of deformed shapes obtained for different values of the pseudo-time parameter is plotted in Fig. 12. (The total value of the loading is reached for the pseudo-time value equal to 10.)

In fact the sequence of the deformed shapes is more complex that it appears from Fig. 12. While the free-end rotation keeps increasing, the out-of-plane displacement takes oscillatory values given in Fig. 13. Each passing through zero in the diagram shown in Fig. 13 roughly corresponds to a beam deformed shape which is entirely situated in the plane. With the increased values of the moment and the force, a new helical deformed shape forms but on the negative side of the out-of-plane axis. The sequence of these deformed shapes is presented in Fig. 14.

We have verified that essentially the same numerical results are obtained with the beam element of Simo and Vu-Quoc [11], employing the orthogonal tensor representation of the finite rotations (see Fig. 13). However, as already pointed out in the previous example, in order to retain the quadratic convergence rate of the Newton iterative scheme with this element the non-symmetric tangent operator must be used, which roughly doubles the computational cost.

The beam element of Ibrahimbegovic et al. [15], employing the total rotation vector, fails in this problem. Namely, as soon as the rotation vector reaches the value equal to 2π, the rank-deficiency of the tangent operator occurs (due to the total rotation vector parameterization singularity, see Section 3) which leads to a divergent response (see Fig. 13). Even in the neighborhood of the singularity point, where the computations can be completed, the tangent operator is ill-conditioned and the obtained results are erroneous. We refer to Fig. 15 for

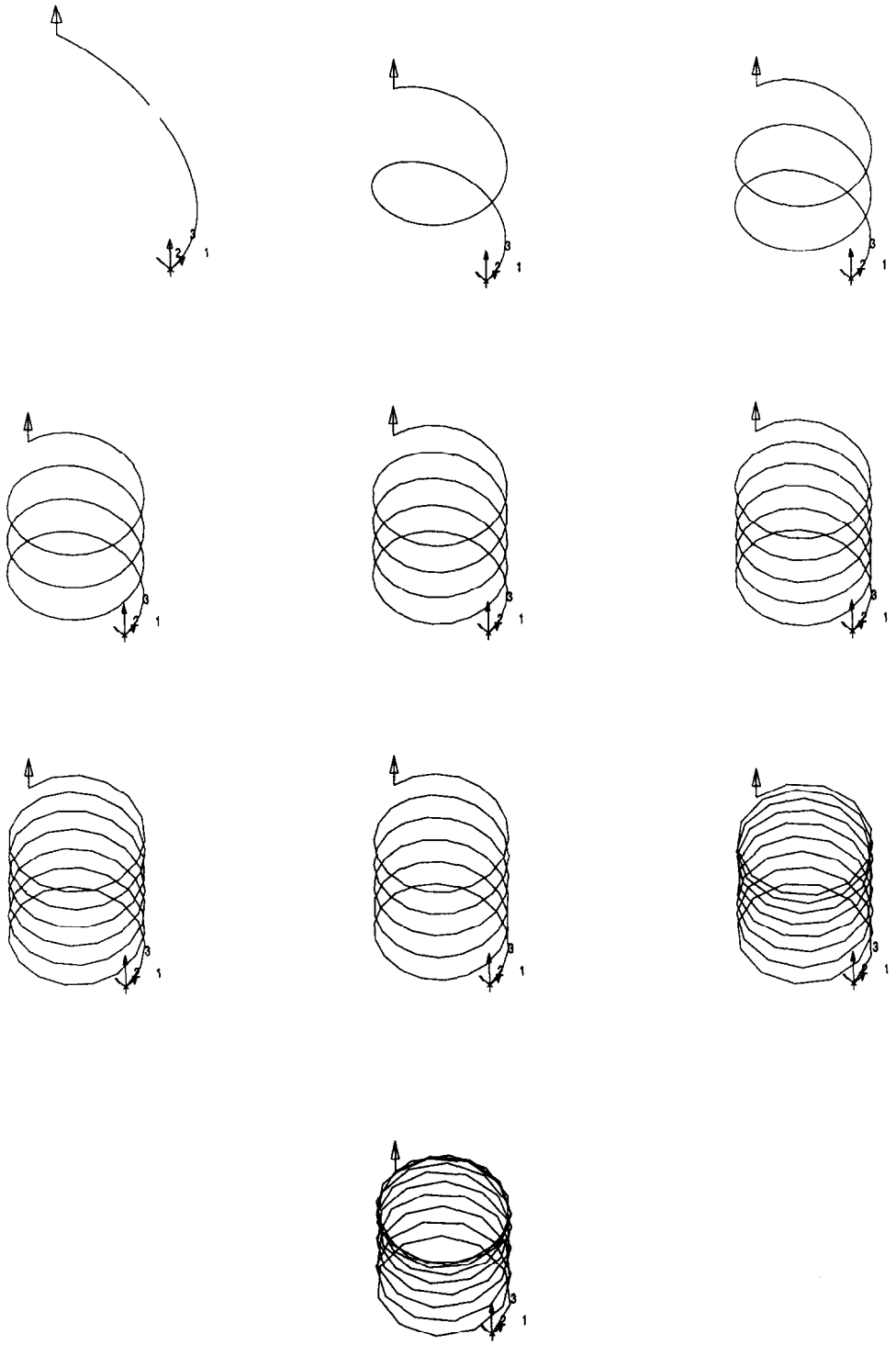

Fig. 12. Deformed shapes of a beam bent in helical form for pseudo-time values equal to: $t = 0.5$, 1.5, 2.5, 3.5, 4.5, 5.5, 6.5, 7.5, 8.5 and 9.5.

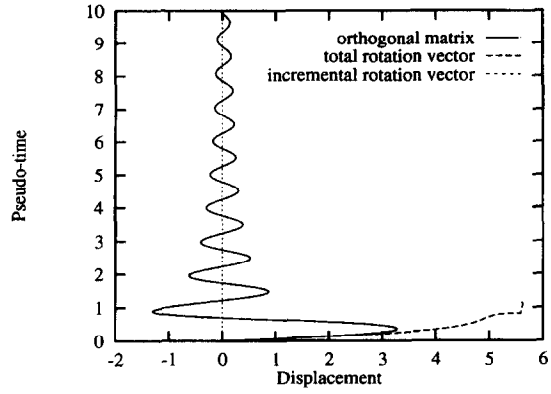

Fig. 13. Free-end displacement component in the direction of applied force.

quite different deformed shapes of this kind computed by the models employing the total and the incremental rotation vectors, respectively.

5.3. Dynamic response of a cantilever beam

In the last example we study the dynamic response of the cantilever beam defined in the first example (see Fig. 11). All the mechanical and geometric characteristics of the beam are kept the same as in the previous example. In addition, we choose the distributed mass per unit length as $A_\rho = 1$ and the moment of inertia of the beam section as $\boldsymbol{J}_\rho = \mathrm{diag}(20, 10, 10)$.

The loading acting on the beam is again the bending moment and the out-of-plane force applied at the free-end, but with the time-variation defined as shown in Fig. 16.

The numerical results for the time-history of the out-of-plane displacement component are obtained with a finite element model of 10 beam elements employing the incremental rotation vector. The computation is performed with the Newmark time-stepping method as described in Section 4. The same computation is performed with a model composed of 10 beam elements of Ibrahimbegovic et al. [15] employing the total rotation vector, in which case the standard implementation of the Newmark scheme can be used. As shown in Fig. 17, two sets of results are essentially the same almost until the end of the time interval of interest.

By looking at the time-history of the norm of the total rotation vector, given in Fig. 18, it is apparent that the discrepancy between these results coincides with increased values of rotation, which provokes an ill-conditioning of the tangent operator in the total vector parameterization.

Closing remarks

In this work we presented a careful treatment of the finite rotations of a geometrically exact beam, employing the incremental rotation vector for rotation parameterization. This choice of parameters eliminates the disadvantages while retaining the advantages of two extreme possibilities for parameterizing the finite rotations, an orthogonal tensor or a rotation vector, in that the tangent operator remains symmetric and the rotation update (within each time step) remains additive, while preventing the tangent operator ill-conditioning problems. Moreover, the proposed rotation parameterization fits naturally within the framework of an iterative solution strategy for nonlinear problems based on one-step integration procedure, allowing for the rejection of the intermediate (non-converged) results and repeated execution in a time step.

The incremental rotation vector also plays a key role in constructing a variant of the Newmark time-stepping scheme for dynamics of finite rotations.

Although we addressed only the model problem of geometrically exact beam, the presented rotation

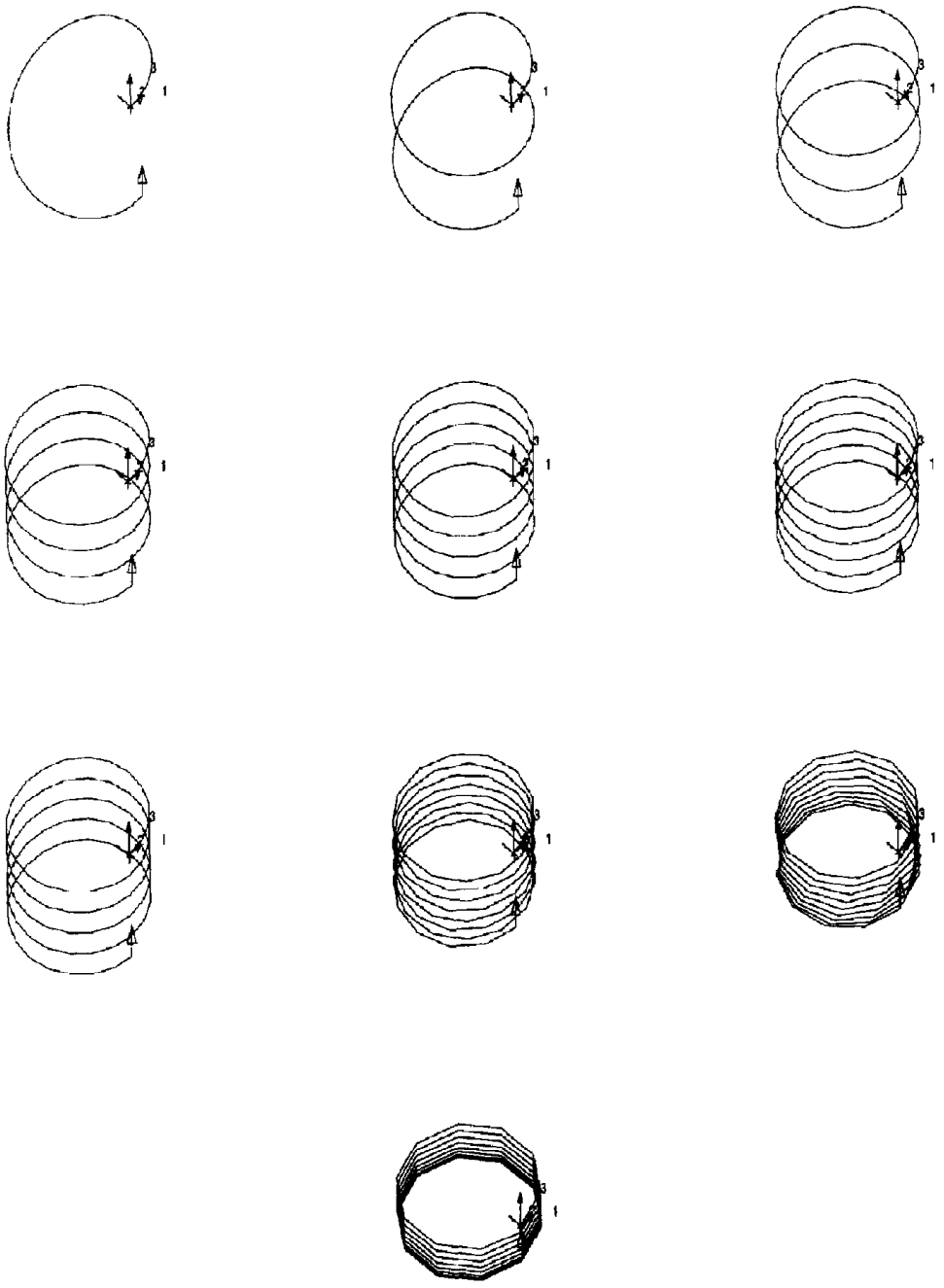

Fig. 14. Deformed shapes of a beam bent in helical form for pseudo-time values equal to $t = 1, 2, 3, 4, 5, 6, 7, 8, 9$ and 10.

parameterization can directly be applied to other structural theories which make use of finite rotations (see e.g. [8, 9]).

Acknowledgements

The financial supports from ABONDEMENT ANVAR and POLE MODELISATION DE PICARDIE are gratefully acknowledged. I am thankful to M. Al Mikdad and P. Courtois for their help in preparing this paper.

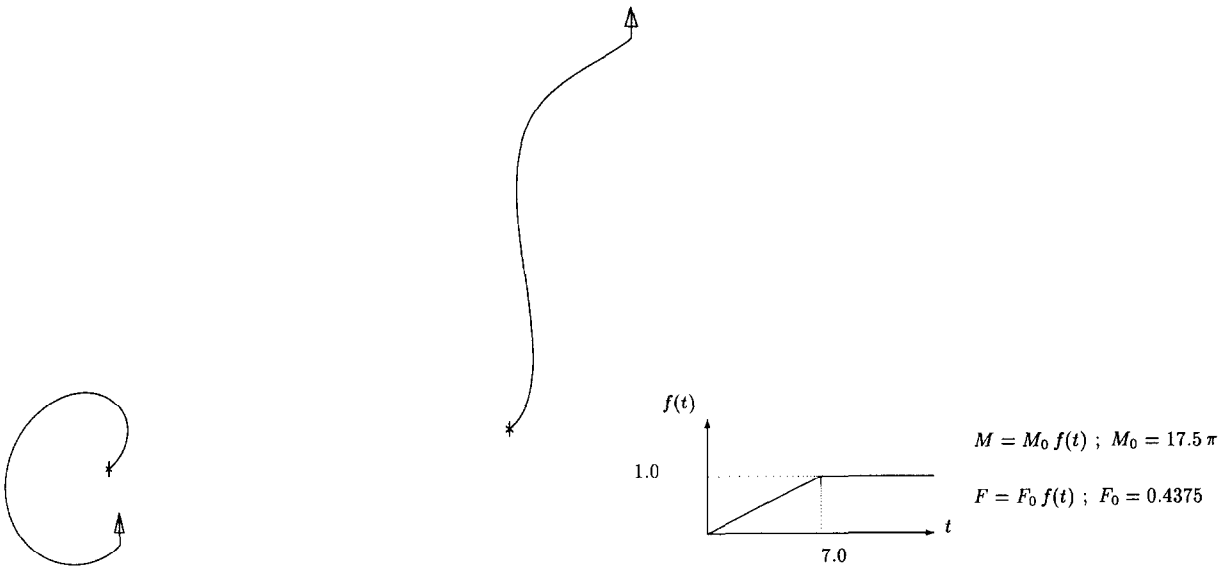

Fig. 15. Deformed shapes computed at $\theta \approx 2\pi$ by the beam models employing incremental and total rotation vector parameters.

Fig. 16. Time-history of applied loads.

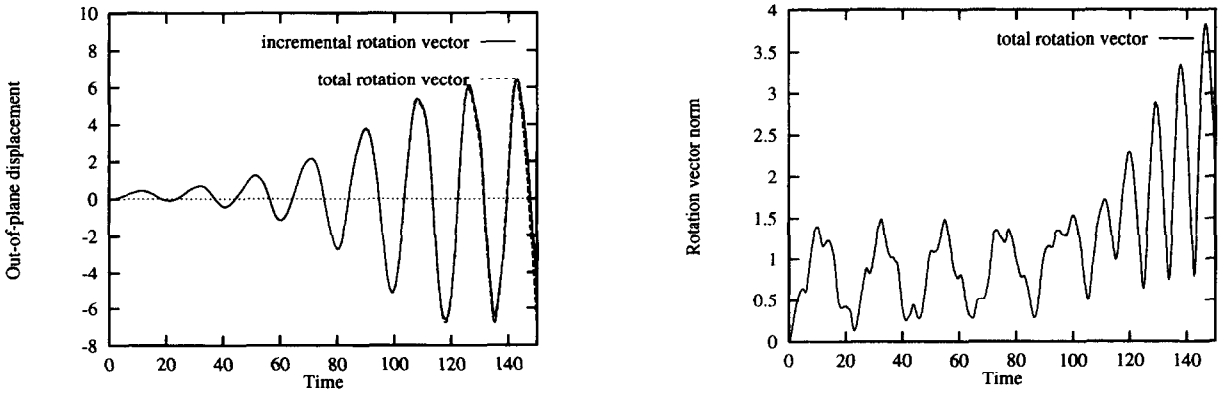

Fig. 17. Time-history of out-of-plane dynamic response.

Fig. 18. Time-history of the total rotation norm.

References

[1] J.T. Oden, Finite Elements of Nonlinear Continua (McGraw-Hill, London, 1972).
[2] J.T. Oden and J.A.C. Martins, Models and computational methods for dynamic frictional contact, Comput. Methods Appl. Mech. Engrg. 52 (1985) 527–634.
[3] J.T. Oden and J.R. Cho, Adaptive *hpq*-finite element of hierarchical models for plate- and shell-like structures, Proc. 3rd USCCM, J.N. Reddy, ed., Dallas, Texas, 67, 1995.
[4] H. Cheng and K.C. Gupta, A historical note on finite rotations, ASME J. Appl. Mech. 56 (1989) 139–145.
[5] Y. Choquet-Bruhat and C. DeWitt-Morette, Analysis, Manifolds and Physics (North-Holland, Amsterdam, 1987).
[6] J.H. Argyris, An excursion into large rotations, Comput. Methods Appl. Mech. Engrg. 32 (1982) 85–155.
[7] J.C. Simo, The (symmetric) hessian for geometrically nonlinear models in solid mechanics: Intrinsic definition and geometric interpretation, Comput. Methods Appl. Mech. Engrg. 96 (1992) 189–200.
[8] A. Ibrahimbegovic, Stress resultant geometrically nonlinear Shell theory with drilling rotations. Part I: A consistent formulation, Comput. Methods Appl. Mech. Engrg. 118 (1994) 265–284.
[9] A. Ibrahimbegovic, Finite elastic deformations of three-dimensional continuum with independent rotation field, in: T.J.R. Hughes et al., eds., Recent Developments in FE Analysis: A book dedicated to R.L. Taylor (CIMNE, Barcelona, 1994) 151–160.
[10] S.S. Antman, Nonlinear Problems in Elasticity (Springer-Verlag, Berlin, 1995).

[11] J.C. Simo and L. Vu-Quoc, A three-dimensional finite-strain model. Part II: Computational aspects, Comput. Methods Appl. Mech. Engrg. 58 (1986) 79–116.
[12] A. Cardona and M. Geradin, A beam finite element non-linear theory with finite rotations, Int. J. Numer. Methods Engrg. 26 (1988) 2403–2438.
[13] C. Sansour and H. Bufler, An exact finite rotation shell theory, its mixed variational formulation and its finite element implementation, Int. J. Numer. Methods Engrg. 34 (1992) 73–115.
[14] N. Buechter and E. Ramm, Shell theory versus degeneration—A comparison in large rotation finite element analysis, Int. J. Numer. Methods Engrg. 34 (1992) 39–59.
[15] A. Ibrahimbegovic, F. Frey and I. Kozar, Computational aspects of vector-like parameterization of three-dimensional finite rotations, Int. J. Numer. Methods Engrg. 38 (1995) 3653–3673.
[16] K.W. Spring, Euler parameters and the use of quaternion algebra in the manipulation of finite rotations: A review, Mech. Mach. Theory 21 (1986) 365–373.
[17] M. Geradin and D. Rixen, Parameterization of finite rotations in computational dynamics: A review, European J. Finite Elem., special issue, A. Ibrahimbegovic and M. Geradin, eds., 4 (1995) 497–553.
[18] S.N. Atluri and A. Cazzani, Rotation in computational solid mechanics, Arch. Comput. Methods Engrg. 2 (1995) 49–138.
[19] J. Stuelpnagel, On the parameterization of the three-dimensional rotation group, SIAM Rev. 6 (1964) 422–430.
[20] A. Ibrahimbegovic, On FE implementation of geometrically nonlinear Reissner's beam theory: Three-dimensional curved beam finite elements, Comput. Methods Appl. Mech. Engrg. 122 (1995) 11–26.
[21] R.A. Spurrier, Comments on 'Singularity-free extraction of a quaternion from a direction-cosine matrix', J. Spacecraf 15 (1978) 255–256.
[22] J.C. Simo and L. Vu-Quoc, On the dynamics in space of rods undergoing large motions: A geometrically exact approach, Comput. Methods Appl. Mech. Engrg. 66 (1988) 125–161.
[23] E. Reissner, On one-dimensional finite-strain beam theory: The plane problem, J. Appl. Math. Phys. 23 (1972) 795–804.
[24] J.L. Ericksen, Tensor fields, in: J. Flugge, ed., Principles of Classical Mechanics and Field Theories, Encyclopedia of Physics, Vol. III/1 (Springer, Berlin, 1960).
[25] P. Germain, La méthode des puissances virutelles en mécanique des milieux continus, J. Mécanique, 12 (1973) 235–274.
[26] J.E. Marsden and T.J.R. Hughes, Mathematical Foundations of Elasticity (Prentice-Hall, Englewoods Cliffs, NJ, 1983).
[27] H. Goldstein, Classical Mechanics (Addison-Wesley, Reading, MA, 1980).
[28] M.F. Beatty, Vector analysis of finite rigid rotations, ASME J. Appl. Mech. 47 (1977) 501–502.
[29] M.W. Hirsch and S. Smale, Differential Equations, Dynamical Systems and Linear Algebra (Academic Press, New York, 1976).
[30] S. Lang, Differential Manifolds (Springer-Verlag, Berlin, 1985).
[31] B. Noble and J.W. Daniel, Applied Linear Algebra (Prentice Hall, Englewood Cliffs, NJ, 1977).
[32] N.M. Newmark, A method of computation for structural dynamics, ASCE J. Engrg. Mech. 112 (1959) 67–94.
[33] A. Ibrahimbegovic and M. Al Mikdad, Finite rotations in dynamics of beams and implicit time-stepping schemes, Int. J. Numer. Methods Engrg. (1996), in press.
[34] O.C. Zienkiewicz and R.L. Taylor, The Finite Element Method: Basic Formulation and Linear Problems, Vol. I (McGraw-Hill, London, 1989).